Comparison Between Two Different Antennas for UWB On-Body Propagation Measurements

A. Alomainy, Y. Hao, *Member, IEEE*, C. G. Parini, *Member, IEEE*, and P. S. Hall, *Fellow, IEEE*

***Abstract*—The effect of two different antenna types on radio propagation in ultrawideband (UWB) on-body channel measurement are analyzed. Statistical path loss parameters and time domain channel characteristics [mean delay and root mean square (rms) delay spread] are extracted from measurement data. Reduction in rms delay spread is experienced when using printed horn shaped self-complementary antennas (HSCA) for specific body area links in comparison to monopole-like omnidirectional antennas, e.g., planar inverted cone antennas (PICA). Results show that the hybrid use of different type UWB antennas can effectively improve channel behavior in body-centric wireless networks.**

***Index Terms*—Frequency domain sounding, on-body channel, ultrawideband (UWB) antenna.**

I. Introduction

BODY-CENTRIC wireless networks are aiming to provide communication systems with constant availability, reconfigurability, unobtrusiveness, and true extension of a human's mind. Such networks have special properties and requirements in comparison to others and that is due to the rapid changes in communication channel behavior on the body during network operation. This raises some important issues regarding the propagation channel characteristics, radio system compatibility, and the effect of the human body. On-body propagation channel characterization for narrowband communication systems has been presented in [1].

Ultrawideband (UWB) communication is a low-power, high-data-rate technology which facilitates the compatibility of such a technology in body-centric network applications [2]. In addition, its low transmit power requirements due to control over duty cycle allows longer battery life for wearable units. Most work on UWB wireless communication channel has been on indoor and outdoor radio propagation modeling and characterization [2] and [3]. The effects of antenna characteristics on indoor UWB propagation channels were investigated and presented in [4] to determine the influence of antenna directionality on the indoor communication channels. UWB on-body channel characterization was presented in [5] only for pre-defined sets of nodes with multi-hopping networking in mind to determine energy and power requirements, however, more realistic representation of the human body behavior such as different body positions and movements were not analyzed.

In this paper, we present a detailed description of the measurement campaign performed in order to obtain sufficient path variation data for acceptable characterization of the UWB on-body channels. Two types of UWB antennas [printed horn shaped self-complementary antennas (HSCA) and planar inverted cone antennas (PICA)] were used to evaluate their effects in the measurement. Effects of different measured channel responses are also highlighted by investigating the received UWB pulses for both antenna cases. Analysis and results show that the application of different antenna types for different on-body links might provide better solution for wireless body-centric networks.

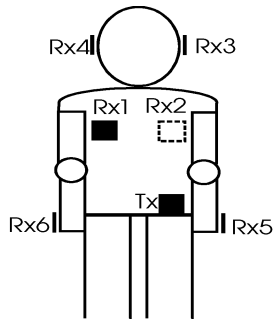

Fig. 1. Antenna positions for on-body propagation channel measurement.

II. On-Body Propagation Channel Measurement

A. Setup

Frequency-domain measurements were performed in the range 3 to 9 GHz with intervals of 3.75 MHz, at a rate of 800 ms, for UWB on-body communication channels. A HP8720ES vector network analyzer (VNA) was used in addition to two pairs of different UWB antennas to measure channel frequency response (S_{21}). The VNA measures the magnitude and phase of each frequency component so that the time domain response can be obtained by means of inverse discrete Fourier transform (IDFT). Two sets of measurements were performed in the anechoic chamber to account for deterministic channel characteristics due to the human body for both antenna types, which resulted in 710 frequency responses for different body positions, Fig. 1. Real human candidates were used for evaluation of the on-body channels. All measurements in this study were taken using effective isotropic radiated power of the order of 0 dBm, which is approximately 30 dB less than that emitted by cell phones during SAR testing. Fifteen frequency sweeps were taken for each on-body channel with the channels being

Manuscript received November 8, 2004; revised December 16, 2004. This work was supported in part by the Engineering and Physical Sciences Research Council.

A. Alomainy, Y. Hao, and C. G. Parini are with the Electronic Engineering Department, Queen Mary, University of London, London E1 4NS, U.K. (e-mail: y.hao@elec.qmul.ac.uk).

P. S. Hall is with the Department of Electronic Engineering, University of Birmingham, Birmingham B15 2TT, U.K.

Digital Object Identifier 10.1109/LAWP.2005.844143

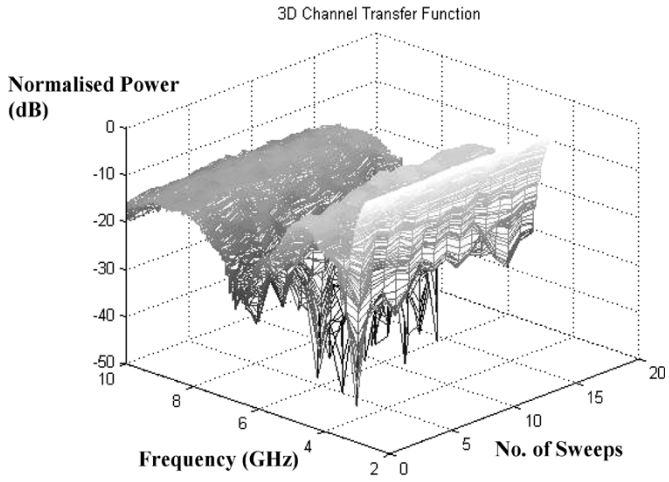

Fig. 2. Normalized three-dimensional channel transfer function at Tx/Rx1 link over 15 sweeps (variations of around 4 dB occurred).

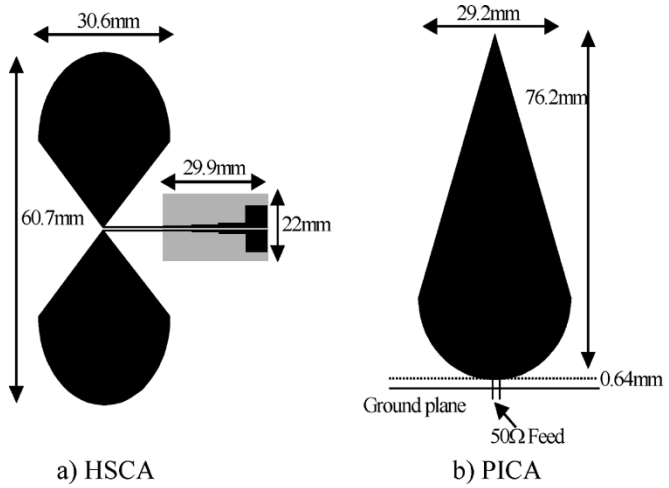

Fig. 3. Layouts of the HSCA and PICA antenna designs with dimensions. (a) HSCA. (b) PICA.

static, Fig. 2. The time domain responses of different frequency sweeps for the specific on-body channel were compared to evaluate the stability of the channel. During measurements, PICA was placed with its cone perpendicular to the body and HSCA was placed with the radiating patch facing outward.

B. UWB Antennas

The UWB antennas (HSCA and PICA) were designed and fabricated following the description outlined in [6] and [7]. The printed HSCA was fabricated on RT/Duroid board with $\varepsilon_r = 3$ and thickness of 1.524 mm. The actual antenna dimensions 30.6 $\times$ 60.7 mm and a 22 $\times$ 29.9 mm ground plane were added for the matching transformer, Fig. 3(a). The HSCA exhibits approximately constant impedance and absolute gain across the UWB band and its gain was found to be between 0 and 2.4 dBi. The antenna radiation patterns experienced some distortions at higher frequencies and produced peaks at directions other than the main beam. This could be due to the substrate thickness and ground plane used for matching circuits causing unexpected radiation. The PICA antenna is derived from the volcano antenna and the circular disk antenna concepts; it is composed of

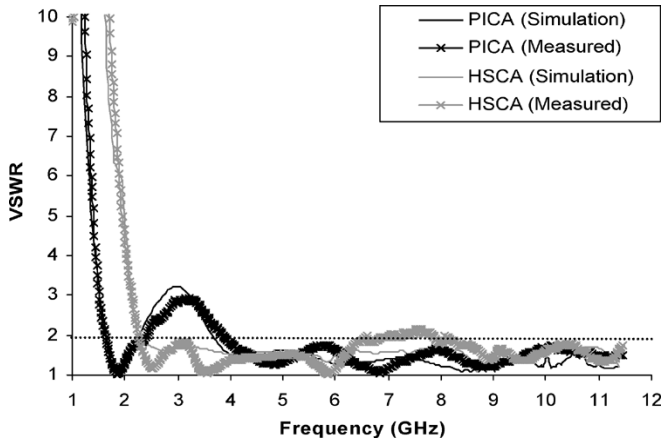

Fig. 4. Simulated and measured VSWR for the PICA and HSCA antennas.

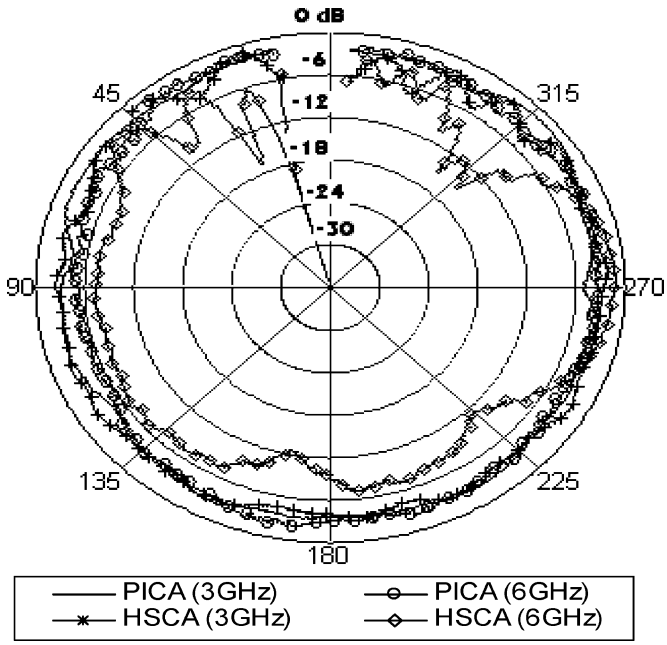

Fig. 5. E-field patterns at 3 GHz and 6 GHz for both antennas (PICA and HSCA).

a single flat element vertically mounted above a small ground plane. The antenna geometry is very simple with an antenna dimension of 29.2 $\times$ 76.2 mm, conductor thickness for the cone around 0.3 and 0.4 mm, and a ground plate dimension of 30 $\times$ 50 mm, Fig. 3(b). The antenna provides outstanding impedance and radiation pattern performance with a gain of 3 to 6 dBi. This configuration was chosen to represent the general omnidirectional monopole-like antennas. Although better cross-polar performance and pattern bandwidth is achieved with the modified design in [7], the PICA applied has much better pattern performance in comparison to HSCA.

Fig. 4 shows the simulated and measured VSWR of both antennas referenced to 50 Ω. VSWR is less than two for the UWB band in the HSCA case; however, for the PICA case, VSWR is less than two starting from 3.7 GHz. Comparison between the radiation patterns of each of the antennas discussed above is shown in Fig. 5 at 3 and 6 GHz. The PICA radiates omnidirectionally across the UWB band. On the other hand, at 6 GHz the

TABLE I
MEAN AND STANDARD DEVIATION OF rms DELAY SPREAD

	HSCA		PICA	
Antenna position	μ_{rms}	σ_{rms}	μ_{rms}	σ_{rms}
Chest (Rx1)	2.47	0.80	2.74	0.39
Back (Rx2)	6.20	2.67	6.67	3.71
Left hand (Rx5)	1.73	1.34	1.87	0.38
Right hand (Rx6)	3.84	2.41	3.19	0.86
Head left side (Rx3)	2.91	1.34	1.91	0.55
Head right side (Rx4)	3.80	1.19	3.36	1.01

All values in nanoseconds (ns)

HSCA radiation pattern exhibits a maximum radiation at 270°, which affects the pattern bandwidth and, hence, the antenna effective bandwidth in comparison to the PICA.

III. MEASUREMENT DATA ANALYSIS

A. Time Domain Results

Channel impulse responses were calculated based on the measured frequency transfer functions which consist of 1601 frequency points using windowing and IDFT. The time domain results for both measurement sets were compared for evaluation. The time domain window can detect multipath signals separated up to 267 ns, which is more than required since no signals were detected higher than 80 ns. Power delay profiles (PDP) were produced by averaging all impulse responses and determining the noise threshold.

The PDP is characterized by the first central moment (mean excess delay $\tau_{\rm m}$) and the square root of the second moment of the PDP [root mean square (rms) delay spread $\tau_{\rm rms}$]. The rms delay spread provides a figure of merit for estimating data rates for multipath channels [8]. From [8], the mean excess delay is defined as

$$\tau_m = \sqrt{\frac{\sum_{i=0}^{N-1} \tau_i . |h(\tau_i)|^2}{\sum_{i=0}^{N-1} |h(\tau_i)|^2}} \tag{1}$$

and the delay spread $\tau_{\rm rms}$ as

$$\tau_{\rm rms} = \sqrt{\frac{\sum_{i=0}^{N-1} (\tau_i - \tau_m)^2 . |h(\tau_i)|^2}{\sum_{i=0}^{N-1} |h(\tau_i)|^2}} \tag{2}$$

A 90 ns interval was considered for delay parameter evaluation, since echoes fade after this threshold. Table I shows a summary of the mean and standard deviation of the rms delay spread $\mu_{\rm rms}$, $\sigma_{\rm rms}$ for both measurement sets. It is obvious that the mean delay due to the Tx/Rx2 (receiving antenna at back) link is the highest where non-line-of-sight channel and propagation guided by the human body (free space wave and surface wave) are the main propagation channels. Reduction in mean rms delay for links with small distances and where human body surface presents a common ground to Tx/Rx in the HSCA antenna case comparing with the PICA (cases Rx1, Rx2, Rx5). For other links where line-of-sight components are the dominant (free space wave) PICA produces a better delay performance. This can be due to the fact that additional radiation is caused by the HSCA board edges, which is being propagated through the human body surface. Fig. 6 shows the rms delay spread versus distance for both measurement cases.

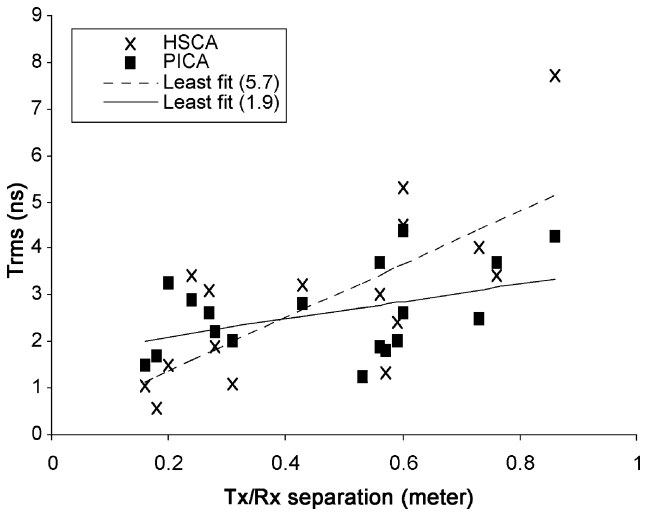

Fig. 6. RMS delay spread versus distance for both HSCA and PICA measurements.

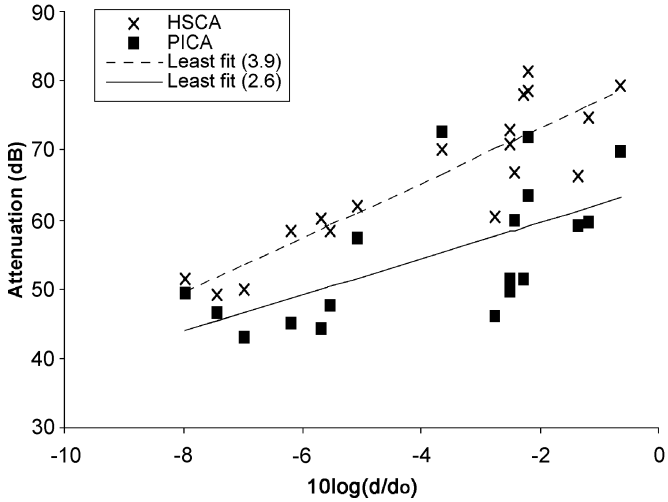

Fig. 7. Path loss for the on-body channels (measured and modeled) for both antenna cases (PICA and HSCA).

B. Path Loss

The path loss of the channel is calculated directly from the measurement data using averages over the measured frequency transfers at each frequency point [4]. It is known that the mean path loss referenced to a distance d_o (reference distance is 1 m as

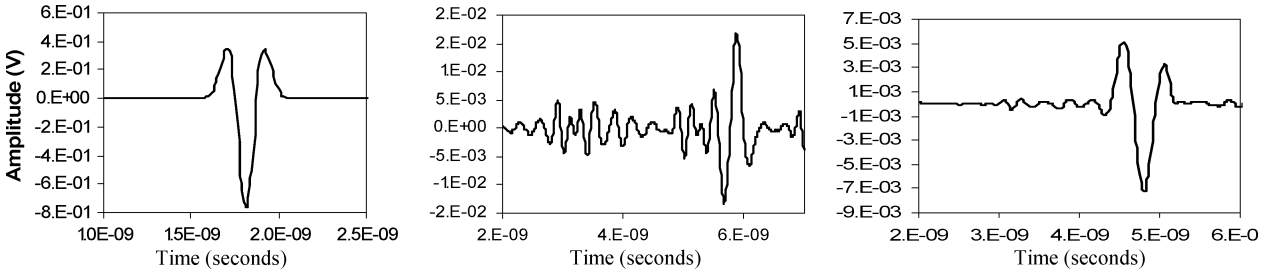

Fig. 8. Transmitted and received pulses of the modeled UWB system with (a) transmitted pulse, (b) received pulse for PICA channel, and (c) received pulse for HSCA channel.

calibrated for VNA measurement) can be modeled as a function of distance using [3]

$$PL_{\mathrm{dB}}(d) = PL_{\mathrm{dB}}(d_o) + 10\alpha \log\left(\frac{d}{d_o}\right) \tag{3}$$

where α is the path loss exponent (loss is presented as a positive value) and $PL_{\mathrm{dB}}(\mathrm{d}_0)$ is the mean path loss at 1 m. A least square fit computation is performed on measured path loss results to get the mean path loss at d_0 and exponent α. Fig. 7 presents the measured values and modeled path loss for both antenna cases. The two types of antennas give different path loss exponents, for the HSCA case $\alpha = 3.9$ and $\alpha = 2.6$ for the PICA. These high exponent values are due to the nonreflecting environment in the anechoic chamber. In the PICA case, the exponent value is higher than the HSCA case and that is due to multipathing from the human body and clothes caused by the PICA excellent omnidirectional radiation and gain across UWB range.

C. Effects on Received UWB Pulses

A system level modeling was performed, in Agilent DSP Designer, to investigate the effect of measured channel responses on received UWB pulses in both antenna cases. Fig. 8 shows the transmitted and received pulses for on-body channel scenario Rx1 (Fig. 1), where the receiver antenna is placed on the right side of the chest. The variation in time delays between the different received pulses highlights the antenna characteristics effect on the channel behavior of the on-body links for the received pulses. More echo and noise components are introduced in the case of pulses received under the PICA measured channel responses compared to the HSCA. However, the improved pulse shape received in the HSCA case is traded off by reduction in energy received in comparison to the PICA.

IV. Conclusion

UWB on-body propagation channel measurements were performed in an anechoic chamber and the deterministic channel characteristics were studied. Two types of UWB antennas were used in order to investigate their effects on the channel behavior. When using the printed HSCA for Tx and Rx, reduction in mean rms delay spread were noticed for cases where surface waves were dominant in the wave travelling along the human body. In contrast, when PICA was used in the same scenarios, the main radiation cone was perpendicular to the body and mean spread delays were higher due to free space wave domination. Path loss analysis and modeling presented non-line-of-sight behavior and this was due to attenuation and shadowing by the human body and the nonreflecting environment. Antenna effects on received UWB pulses presented more distortion in pulses received when the PICA channel results were applied in the system modeling and this could be due to the presence of nulls in HSCA radiation.

Acknowledgment

The authors would like to thank X. Hu and W. Dong for their help and assistance with the measurements.

References

[1] Y. Nechayev, P. Hall, C. C. Constantinou, Y. Hao, A. Owadally, and C. G. Parini, "Path loss measurements of on-body propagation channels," in *Proc. 2004 Int. Symp. Antennas and Propagation*, Sendai, Japan, pp. 745–748.

[2] (2004) Proc. IEEE Vehicular Tech. Conf. (VTC2004-Fall), Los Angeles, CA. [Online]. Available: http://www.see.ed.ac.uk/~ccc/research.html

[3] S. S. Ghassemzadeh, R. Jana, C. W. Rice, W. Turin, and V. Tarokh, "A statistical path loss model for in-home UWB channels," in *Proc. IEEE Conf. Ultra Wideband Systems and Technologies, UWBST*, Baltimore, MD, 2002, pp. 59–64.

[4] J. A. Dabin, N. Ni, A. M. Haimovich, E. Niver, and H. Grebel, "The effects of antenna directivity on path loss and multipath propagation in UWB indoor wireless channels," in *Proc. IEEE Conf. Ultra Wideband Systems and Technologies*, Newark, NJ, 2003, pp. 305–309.

[5] T. Zasowski, F. Althaus, M. Stager, A. Wittneben, and G. Troster, "UWB for noninvasive wireless body area networks: channel measurements and results," in *Proc. IEEE Conf. Ultra Wideband Systems and Technologies*, Reston, VA, 2003, pp. 285–289.

[6] A. Saitou, T. Iwaki, K. Honjo, K. Sato, T. Koyama, and K. Watanabe, "Practical realization of self-complementary broadband antenna on low-loss resin substrate for UWB applications," in *Proc. 2004 IEEE MTT-S Int. Microwave Symp.*, Fort Worth, TX, 2004, pp. 1263–1266.

[7] S.-Y. Suh, W. L. Stutzman, and W. A. Davis, "A new ultrawideband printed monopole antenna: the Planar Inverted Cone Antenna (PICA)," *IEEE Trans. Antennas Propag.*, vol. 52, no. 5, pp. 1361–1364, May 2004.

[8] T. S. Rappaport, *Wireless Communications: Principles and Practice*. Englewood Cliffs, NJ: Prentice-Hall, 1999.